Supplementary Information

Highly durable superhydrophobic activated biochar catalyst for biodiesel synthesis: Process optimization and economic feasibility analysis

Arpita Das [a], Chandrakanta Guchhait [b], Bimalendu Adhikari [b], Hui Zhou [c], Bidhan Kumbhakar [d], Xianzhi Meng [e], Hu Li [f], Samuel Lalthazuala Rokhum [a*]

[a] *Department of Chemistry, National Institute of Technology Silchar, Silchar, 788010, India*

[b] *Department of Chemistry, National Institute of Technology Rourkela, Rourkela, Odisha, 769008, India*

[c] *Department of Energy and Power Engineering, Room A218, Tsinghua University, Beijing 100084, China*

[d] *Department of Chemical and Biological Sciences, S. N. Bose National Centre for Basic Sciences, Kolkata, 700106, India*

[e] *Department of Chemical and Biomolecular Engineering, University of Tennessee Knoxville, Knoxville, TN 37996, USA*

[f] *State-Local Joint Laboratory for Comprehensive Utilization of Biomass Center for R&D of Fine Chemicals of Guizhou University, Guiyang 550025, China*

[*]Corresponding author's email: rokhum@che.nits.ac.in (SLR)

1. Schematic representation of triglyceride transesterification for biodiesel production

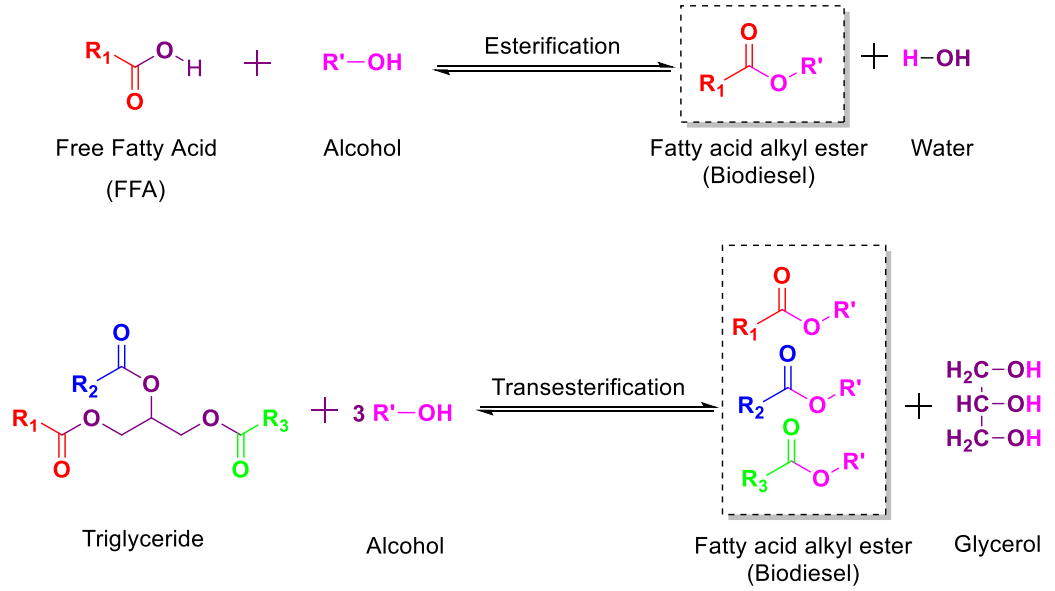

Fig. S1. Transesterification of triglyceride in vegetable oil to biodiesel.

2. Plausible mechanism illustrating breakdown of ester bond in SSAC@PHSO$_3$H

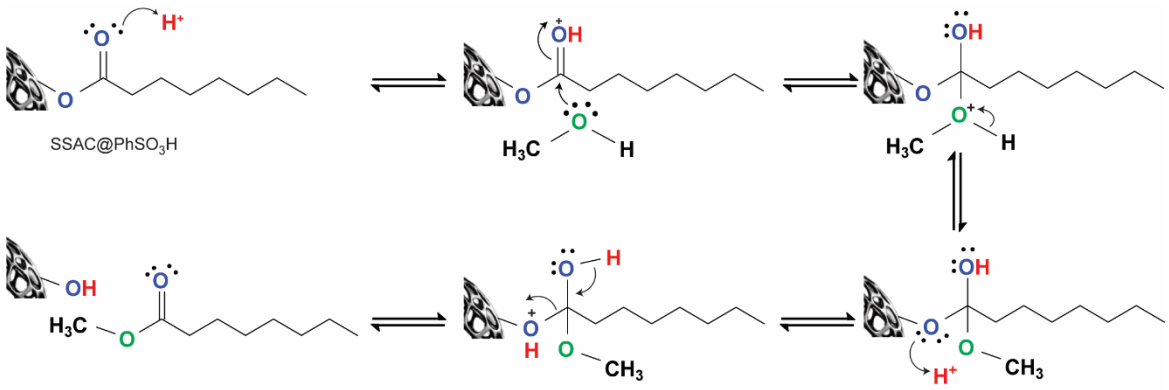

Fig. S2. Mechanistic insight into the ester bond cleavage of SSAC@PhSO$_3$H in acidic environment.

3. Grafting of alkyl chain via Williamson's ether synthesis reaction

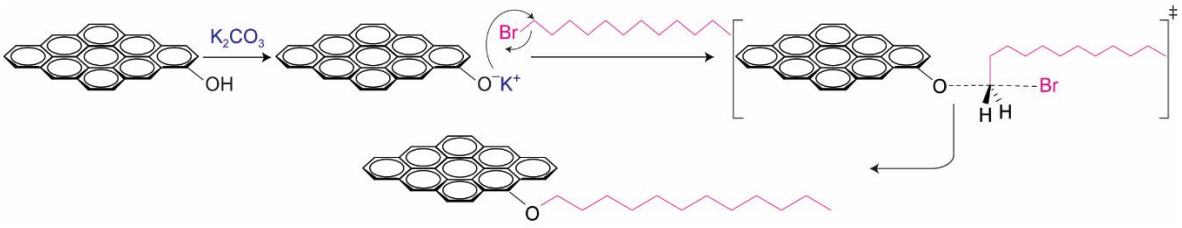

Fig. S3: Grafting of alkyl chain onto biochar surface-Williamson's ether synthesis reaction

4. Steps involved in catalyst preparation

The superhydrophobic acidic biochar catalyst (ESAB@PhSO$_3$H) was synthesized through a sequential three-step process (*please refer to* ***Fig. 2*** *in the manuscript*) involving:

Step 1: Carbonization that includes both hydrothermal carbonization (HTC) and chemical activation using ZnCl$_2$.

Cellulose (8 g) was hydrothermally carbonized in 120 mL deionized water at 190 °C for 20 h in a 200 mL Teflon-lined stainless-steel autoclave. After cooling to room temperature, the slurry was recovered by vacuum filtration (using fritted funnel, G4), washed with deionized water five times, and oven-dried (80 °C, 24 h) to yield cellulose-derived spherical hydrochar (SHC, yield of 62.5%). For activation, SHC was impregnated with $ZnCl_2$ (1:1 wt. ratio), concentrated at 80 °C, dried overnight (100 °C), and carbonized in a tubular furnace under N_2 flow (40 mL min^{-1}) at 500 °C for 2 h. The cooled product was acid-soaked (2 M HCl, 50 mL, 5–6 h), rinsed to neutrality (confirming the absence of chloride ions by silver nitrate test) while the complete removal of Zn^{2+} ions was verified using the potassium ferrocyanide test and dried at 80 °C to yield porous spherical activated biochar (SAB), with a yield of ~ 20%).

Step 2: Sulfonation employing 4-BDS in the ratio of 1:2 to biochar.

The sulfonated activated carbon (SAB@PhSO$_3$H) was obtained by the reaction of 4-benzenediazonium sulfonate (4-BDS) with SAB, using hypophosphorous acid (H_3PO_2) as the reducing agent [1]. The 4-BDS precursor was synthesized via diazotization of 4-aminobenzenesulfonic acid (sulfanilic acid). Briefly, sulfanilic acid (2.165 g) was dispersed in a mixture of HCl (10 mL) and deionized water (10 mL) and stirred at room temperature for 30 min. The suspension was then cooled in an ice bath (0–3 °C) under continuous stirring,

followed by dropwise addition of $NaNO_2$ solution (20 mL, 0.75 M) until a clear solution was obtained. Stirring was continued for an additional 1 h at the same temperature, during which a white precipitate of 4-BDS formed. The product was isolated by filtration (Whatman filter paper), washed repeatedly with cold deionized water three times and acetone, and dried overnight under refrigeration.

For surface functionalization, 4-BDS (2 g) was dispersed in a solvent mixture of deionized water (35 mL) and ethanol (25 mL) at 0–5 °C under stirring for 5–10 min, forming a colloidal suspension. SAB (1 g) was then added, followed by the introduction of 30 mL of 30–32 % hypophosphorous acid (H_3PO_2) as a reducing agent. After 30 min of stirring, an additional 20 mL of H_3PO_2 was added, and the mixture was allowed to stand for 1 h with intermittent agitation until nitrogen gas evolution ceased. The resulting sulfonated carbon (SAB@$PhSO_3H$) was recovered by thorough washing with deionized water (at least 7 times) and acetone, and subsequently dried at 80 °C overnight.

Step 3: Hydrophobization of the sulfonated activated biochar via etherification, followed by acidification

Cellulose-based biochar, rich in hydroxyl groups along its backbone, provides potential sites for chemical modification, particularly hydrophobization. Etherification was employed for cellulose hydrophobization. In a novel synthesis, SAB@$PhSO_3H$ (1 g), K_2CO_3 (1 g) are introduced into a 250 mL round bottom flask containing 40–50 mL dry DMF and subjected to magnetic stirring at 80 °C for 2 h until K_2CO_3 dissolves partially (**Fig. 2)**. Then to the reaction mixture, a pinch of KI is added with 3 mL of 1-Bromododecane (closing mouth of RB with cork), continued stirring at 80 °C overnight, under inert atmosphere (N_2 gas). K_2CO_3 created a mild basic environment, triggering the deprotonation of biochar's phenolic OH group into a potent phenoxide ion, which acted a nucleophile for the 1-Bromododecane, while KI promoted the etherification reaction as a nucleophilic catalyst. The reaction mixture was then filtered using filter paper and washed with acetone (3×10 mL) and water (4×20 mL); the former removes the greasiness of 1-Bromododecane, and the latter removes excess or unreacted K_2CO_3 and KI.

During this etherification step, the sulfonic acid groups (–SO_3H) were deprotonated to sulfonate anions (–SO_3^-) due to the basic environment generated by K_2CO_3. To regenerate the catalytically active sulphonic acid group of the catalyst, a subsequent acidification step was employed (**Fig. 2**). The obtained biochar was acidified by soaking it in 2 M HCl (40 mL)

overnight which effectively converts sulfonate anion into sulfonic acid, to finally obtain the desired catalyst (ESAB@$PhSO_3H$).

5. Details of the instrument employed for catalyst and biodiesel characterization

On a Micromeritics ASAP 2010 surface area and porosity detector, catalyst was degassed for 10 h at 150 ºC before being examined using the BET method. The N_2 adsorption-desorption isotherms were calculated using a Micromeritics ASAP 2010 surface area and porosity analyzer. Thermo gravimetric analysis (TGA) was operated on a PerkinElmer TGA 4000 instrument under the following operating conditions: sample was placed in a very tiny crucible of silica under constant N_2 flow with rate of heating 0.1–200 ºC min^{-1}, and weight loss was measured between 30 and 800 ºC. The samples were heated at a rate of 5 °C min^{-1} using a flow of helium (100 cm^3 min^{-1}). Raman spectroscopy was operated on Witec Alpha300 Confocal Raman Microscope, 355 nm). For powder X-ray diffraction (PXRD), Cu Kα radiation with 2θ = 10–60° was used on a PANalytical X'Pert Pro diffractometer where 40 kV and 100 mA were the operating voltage and current, respectively. The catalyst's functional groups were characterized using a 3000 Hyperion Fourier transform infrared spectroscopy (FTIR) instrument (Bruker, Germany). Scanning Electron Microscopy (SEM) for morphological study and Energy dispersive X-ray Spectroscopy (EDS) study for elemental composition of catalyst were executed on an HR-SEM instrument (FEI Novanano SEM 450 apparatus working subject to conditions: 1.0 nm resolution with platinum nanoparticles mounted on a carbon substrate, that has a FEG assembly source with Schottky emitter (1 to 15 kV Electron Gun), and magnifying power of 35 X–10^6 X). EDS was conducted with a solid angle of 0.28 sr by shifting to EDS mode. Transmission Electron Microscopy (TEM) images as well as selected area electron diffraction (SAED) pattern were recorded in FEI Tecnai f30s twin instrument with magnifications ranging from 2000X to 1500000X. Catalyst was dissolved in ethanol and drop cast onto a Cu grid TEM, which was followed by oven drying. The compound was spread out on carbon tape to be examined. On a PHI 5000 VersaProbe III apparatus with a micro-focused dual-anode Al/Mg K-source monochromated Al K X-ray sources, X-ray photoelectron spectroscopy (XPS) was performed. Likewise, Catalyst hydrophobic nature was determined using a drop shape analyzer (KRUSS, DSA25, Germany) contact angle goniometer. ^{13}C-CP-MAS NMR spectra were measured at room temperature using a Bruker ASX-200 spectrometer at a Lamor frequency of 50.3 MHz. A Bruker MAS probe head was used with a 7 mm zirconia rotor. The spinning rate of the sample was 4.0kHz. The frequency of the spectra is expressed with respect to pure tetramethylsilane. Glycine was used as a second reference material, with

a carbonyl signal set at 176.48 ppm. Temperature-programmed desorption (TPD) was exploited to determine the acidity and strength of the catalyst's surfaces using NH_3 as a probe molecule using a thermal conductivity detector (TCD)-equipped ChemiSorb 2720 analyzer. To eliminate water from the catalysts, the samples underwent a pretreatment under N_2 at 200 ºC for 1 h. Using a ramping rate of 10 °C min^{-1} to 800 ºC under argon, the samples were heated after being purged with N_2 and saturated with 5 mL min^{-1} of pure ammonia for 30 min at 25 °C.

For biodiesel characterization, ^{13}C NMR and ^{1}H NMR data were recorded employing Bruker spectrometer with frequencies of 100 MHz and 400 MHz respectively. Tetramethyl-silane (TMS) and $CDCl_3$ were respectively used as an internal reference and solvent. In addition, to detect the biodiesel constituent, Shimadzu (GC-2030) series GC-MS equipped with Headspace (HS-20) & QQQ Mass spectrometer GC-TQ8040NX was used.

Biodiesel yield i.e., oil conversion to biodiesel and FAME content in percentage were estimated using **Eq. S1** and **S2** respectively.

$$\text{Biodiesel yield or JCO conversion (\%)} = \left(\frac{\text{amount of biodiesel produced}}{\text{amount of oil used}}\right) \times 100 \quad \text{S1}$$

$$\text{FAME content in biodiesel (\%)} = 100 \times \frac{2A_{OMe}}{3A_{\alpha-CH_2}} \quad \text{S2}$$

where, factors 2 and 3 correspond to protons attached with α-carbonyl methylene and methoxy carbons, respectively. A_{OMe} = methyl esters' methoxy groups integration value, $A_{\alpha-CH_2}$ = integral measure of α-carbonyl methylene groups in methyl ester.

6. Modified Ning and Niu's method to ascertain sulfonic groups' density via acid-base titration

Following Ning and Niu's modified method of acid-base titration sulfonic groups' density was calculated (**Eq. S3**) [2]. In this typical procedure, 40 mg catalyst was added to 20 mL, 0.1 M NaCl solution, agitated for 24 h. A quantitative filter paper was used to separate solids from the suspension, and the filtrate was titrated against 0.01 M NaOH using phenolphthalein as pH indicator.

$$\text{Acid density, } C_{SO_3H} = \frac{C_{NaOH} \times V_{NaOH}}{m_c} \quad \text{S3}$$

C_{SO_3H} represents sulfonic group density in mmol g^{-1}; C_{NaOH} stands for NaOH solution concentration in mol L^{-1}; V_{NaOH} is the volume of NaOH required (in mL); and m_c denotes catalyst mass in gram.

7. Reaction kinetics and thermodynamics

Rate of the reaction ($-r_{JCO}$) can be expressed as:

$$-\mathrm{r_{JCO}} = -\frac{\mathrm{d[JCO]}}{\mathrm{dt}} = \mathrm{k[JCO]}$$

herein, [JCO], k and t denote concentration of JCO, rate constant and reaction time respectively. The rate constant (k) was estimated from x_t, the fraction of JCO methyl ester formed over time (t) using **Eq. S4**.

$$-\ln(1-\mathrm{x_t}) = \mathrm{kt} \qquad \text{S4}$$

Activation energy (E_a) was determined employing the Arrhenius equation by substituting rate constants obtained at temperatures ranging from 50–80 °C. A plot of ln k versus 1/T (**Eq. S5**) provided the slope $-E_a/R$ and intercept ln A.

$$\ln\mathrm{k} = \ln\mathrm{A} - \mathrm{E_a/RT} \qquad \text{S5}$$

Here, T, A and R denote absolute reaction temperature (K), pre-exponential factor and universal gas constant (8.314×10^{-3} J K^{-1} mol^{-1}) respectively.

Considering the investigation of the transesterification of JCO utilizing the ESAB@$PhSO_3H$ catalyst at varied temperatures, the thermodynamic characteristics, encompassing the change in enthalpy ($\Delta H^{\ddagger}$), entropy ($\Delta S^{\ddagger}$), and Gibbs free energy ($\Delta G^{\ddagger}$), were evaluated by the Eyring-Polanyi equation (**Eq. S6**) and the Gibbs free energy equation (**Eq. S7**).

$$\ln\frac{\mathrm{k}}{\mathrm{T}} = \frac{\Delta\mathrm{S}^{\ddagger}}{\mathrm{R}} - \frac{\Delta\mathrm{H}^{\ddagger}}{\mathrm{RT}} + \ln\frac{\mathrm{k_b}}{\mathrm{h}} \qquad \text{S6}$$

$$\Delta\mathrm{G}^{\ddagger} = \Delta\mathrm{H}^{\ddagger} - T\Delta\mathrm{S}^{\ddagger} \qquad \text{S7}$$

Here, h and k_b denotes Planck's constant (6.626×10^{-34} J s) and Boltzmann's constant (1.38×10^{-23} J K^{-1}) respectively.

8. Vibrational frequencies and their corresponding bonds from FTIR spectra

Table S1: Vibrational frequencies of SAB@$PhSO_3H$ and ESAB@$PhSO_3H$

Bonds	**Frequencies (cm^{-1})**	
	SAB@$PhSO_3H$	ESAB@$PhSO_3H$
O–H stretching	3380	3371
C–H stretching	-	2916, 2854
C–H bending	-	1396
C–O stretching	1002	1004
C=C stretching	1589	1597
C–O–C stretching	–	1211
β-(1,4)-glycosidic linkage		
S=O (–SO_3H) stretching	1350	1346
	1165	1157
C=O (carbonyl)	1697	1697

9. Acidity profile of fresh and reused ESAB@$PhSO_3H$ catalyst from NH_3-TPD analysis

Table S2: Acidity values of fresh and reused ESAB@$PhSO_3H$ catalyst

Catalyst	Total acid density (mmol g^{-1})	Weak acid density (mmol g^{-1})	Strong acid density (mmol g^{-1})
ESAB@$PhSO_3H$	6.11	2.12	3.99
Reused ESAB@$PhSO_3H$	5.59	2.03	3.56

10. XPS broad survey scan spectra

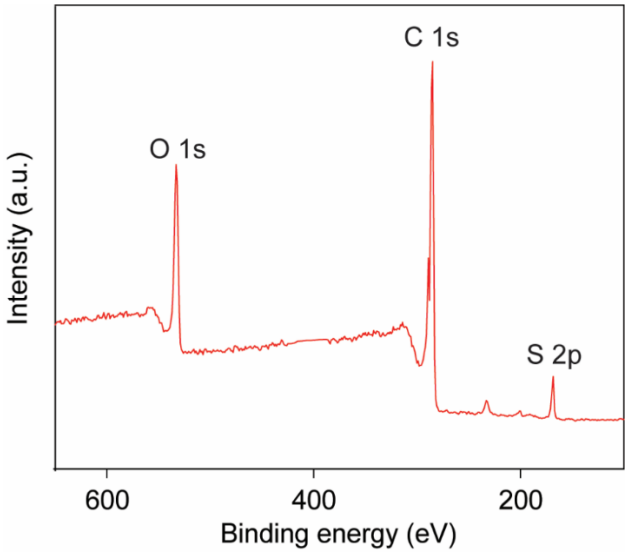

Fig. S4: Overall XPS survey spectrum of ESAB@PhSO$_3$H.

11. EDS spectra and elemental composition of fresh catalyst

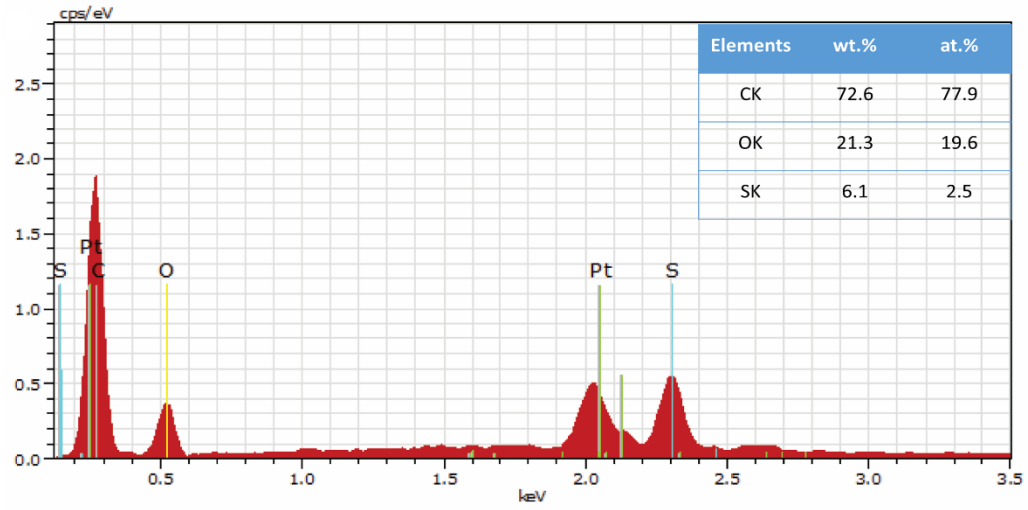

Fig. S5: EDS spectra with elemental composition table (inset) of fresh ESAB@PhSO$_3$H catalyst.

12. Design of experiments for modelling biodiesel yield based on RSM-CCD method

Table S3: Design matrix, including experimental variables (A–D), predicted and actual biodiesel yield for JCO transesterification

Run	Space Type	Factors				Biodiesel yield (%)		Residual
		Catalyst loading (%)	Temperature (°C)	Time (min)	MOMR	Actual	Predicted	
		A	B	C	D			
1	Factorial	7	70	30	20	78.5	79.32	-0.8167
2	Axial	6	60	40	15	81.2	80.52	0.6792
3	Factorial	7	70	30	10	81.1	81.2	-0.0958
4	Factorial	7	90	50	20	89.7	89.92	-0.2167
5	Factorial	5	90	30	10	79.2	79.96	-0.7625
6	Factorial	5	70	50	10	78.3	78.9	-0.5958
7	Factorial	5	70	50	20	77.4	77.12	0.2833
8	Factorial	7	90	30	10	88.1	88.72	-0.6167
9	Center	6	80	40	15	98.6	98.28	0.3167
10	Factorial	7	90	50	10	93.1	93.45	-0.3458
11	Axial	8	80	40	15	92.9	91.97	0.9292
12	Factorial	5	90	50	20	80.2	81.11	-0.9125
13	Factorial	5	90	30	20	71.5	71.38	0.1167
14	Center	6	80	40	15	98.9	98.28	0.6167
15	Factorial	7	70	50	10	89.4	89.85	-0.45

16	Axial	6	100	40	15	92.7	92.04	0.6625
17	Factorial	7	70	50	20	90.3	90.55	-0.2458
18	Center	6	80	40	15	97.9	98.28	-0.3833
19	Factorial	5	90	50	10	87.6	87.12	0.4833
20	Axial	6	80	40	5	87.4	86.82	0.5792
21	Center	6	80	40	15	97.8	98.28	-0.4833
22	Axial	4	80	40	15	70.2	69.79	0.4125
23	Factorial	5	70	30	10	67.7	67.82	-0.1167
24	Factorial	5	70	30	20	62.8	63.46	-0.6625
25	Center	6	80	40	15	98.3	98.28	0.0167
26	Axial	6	80	40	25	79.7	78.94	0.7625
27	Axial	6	80	20	15	67.4	66.39	1.01
28	Factorial	7	90	30	20	82.2	82.61	-0.4125
29	Axial	6	80	60	15	85.1	84.77	0.3292
30	Center	6	80	40	15	98.2	98.28	-0.0833

13. Range and levels of the independent variables

Table S4: Experimental parameters and variable levels utilizing the CCD approach

Variable	Variable Code	Unit	Ranges and levels		
			-1	**0**	**+1**
Catalyst loading	A	wt.%	5	6	7
Temperature	B	°C	70	80	90
Time	C	min	30	40	50
MOMR	D	mol/mol	10	15	20

14. Formulation of regression model

Table S5 depicts the establishment of a regression model based on the experimental yield. The quadratic model was deemed the most appropriate among the fitted models (linear, 2FI, quadratic, and cubic polynomial) for the response variable, owing to its highest polynomial order with signification of additional terms (high F value, lower p-value, and high R^2) and the model was not aliased, rather, suggested by the RSM software.

Table S5: Statistical information for the JCO transesterification proposed models

Source	Sequential p-value	Lack of Fit p-value	Adjusted R^2	Predicted R^2	
Linear	0.0014	< 0.0001	0.4139	0.3839	
2FI	0.9856	< 0.0001	0.2647	0.1359	
Quadratic	**< 0.0001**	**0.0504**	**0.9944**	**0.9844**	**Predicted**
Cubic	0.9417	0.006	0.991	0.7282	**Aliased**

15. Parametric optimum values and contribution percentage for JCO conversion (%)

Table S6 summarizes the parameters as per their contribution percentage. Exploiting the model and individual parameter sum of squares, contribution factors were determined using **Eq. S8** to assess each variable's influence on biodiesel yield.

$$\text{Contribution factor (\%)} = \frac{SS_f}{SS_T} \times 100 \quad \text{S8}$$

where, SS_f= sum of squares of a specific factor, SS_T= sum of squares of the model.

Table S6: Optimum values and contribution percentage of reaction parameters in JCO transesterification

Parameters	Contribution factor (%)	Optimum value
Catalyst loading (% w/w)	23.82	6.14
Temperature (°C)	6.42	78.02
Time (min)	16.36	41.8
MOMR	3.0	14.07

16. Proposed quadratic model's ANOVA outcomes based on RSM-CCD

Adequacy of the quadratic model adopted for the RSM-CCD design was assessed through statistical analysis of variance (ANOVA). Results summarized in **Table S7** indicates a p-value <0.0001, suggesting a mere 0.01 % likelihood that the proposed model values were obtained fortuitously, supported by a high F-value (Fischer's exact test) of 366.51, ensuring reliability of the results i.e., the model is significant at 95 % confidence level. The descending F-values for linear terms, catalyst amount (A), time (C), temperature (B) and MOMR (D) indicate contributions to JCOME yield respectively. CV of ~ 0.92%, less than the allowed value (10 %) suggests extraordinary precision, whilst lack of fit with a p-value 0.05 > 0.01 indicates insignificance, affirming the model fits well with experimental data and accounts for all contributions in the regression response relationship. Furthermore, difference of R^2 values for predicted and adjusted data (0.9844 and 0.9944, respectively) by < 0.01, demonstrates strong correlation between experimental and theoretical data, enabling precise exploration of the design space. Additionally, the high R^2 predicted value indicates good model fitting for JCOME yield prediction with new observations. Moreover, the model's adequate precision (AP) value of 63.37 exceeds the minimal requisite 4, suggesting accurate experimental results and a high signal-to-noise ratio (SNR).

Table S7: Statistical ANOVA result for transesterification of JCO.

Source	Sum of Squares	df	Mean Square	F-value	p-value	Remarks	Accuracy test	
							Parameters	Value
Model	3098.37	14	221.31	366.51	< 0.0001	significant	R^2	0.9971
A	738.15	1	738.15	1222.44	< 0.0001		Adjusted R^2	0.9944
B	198.95	1	198.95	329.48	< 0.0001		Predicted R^2	0.9844
C	506.92	1	506.92	839.5	< 0.0001		Adequate Precision	63.3717

D	93.22	1	93.22	154.38	< 0.0001		Std. Dev.	0.7771
AB	21.39	1	21.39	35.42	< 0.0001		Mean	84.78
AC	5.88	1	5.88	9.74	0.007		C.V.%	0.9166
AD	6.13	1	6.13	10.14	0.0061			
BC	15.41	1	15.41	25.51	0.0001			
BD	17.85	1	17.85	29.56	< 0.0001			
CD	6.63	1	6.63	10.98	0.0047			
A^2	519.27	1	519.27	859.95	< 0.0001			
B^2	247.03	1	247.03	409.1	< 0.0001			
C^2	883.68	1	883.68	1463.45	< 0.0001			
D^2	406.78	1	406.78	673.66	< 0.0001			
Residual	9.06	15	0.6038					
Lack of Fit	8.19	10	0.8189	4.72	0.0504	not significant		
Pure Error	0.8683	5	0.1737					
Cor Total	3107.43	29						

Eq. S9 denotes the predicted response yield, Y_{pre}, derived using quadratic equation. Positive coefficients indicate an enhancement in JCOME yield, while negative coefficients indicate an adverse effect.

$$Biodiesel\ yield, Y_{pre}(\%) = 98.28 + 5.55A + 2.88B + 4.60C - 1.97D - 1.16AB - 0.6062AC + 0.6188AD - 0.9812BC - 1.06BD + 0.6438CD - 4.353A^2 - 3.00B^2 - 5.68C^2 - 3.85D^2 \quad \text{S9}$$

where A, B, C and D are the individual effects of each parameter. AB, AC, AD, BC, BD and CD are the interaction terms. A^2, B^2, C^2 and D^2 are square terms.

17. Diagnostic plot and numerical optimization result for FAME production based on the RSM-CCD method

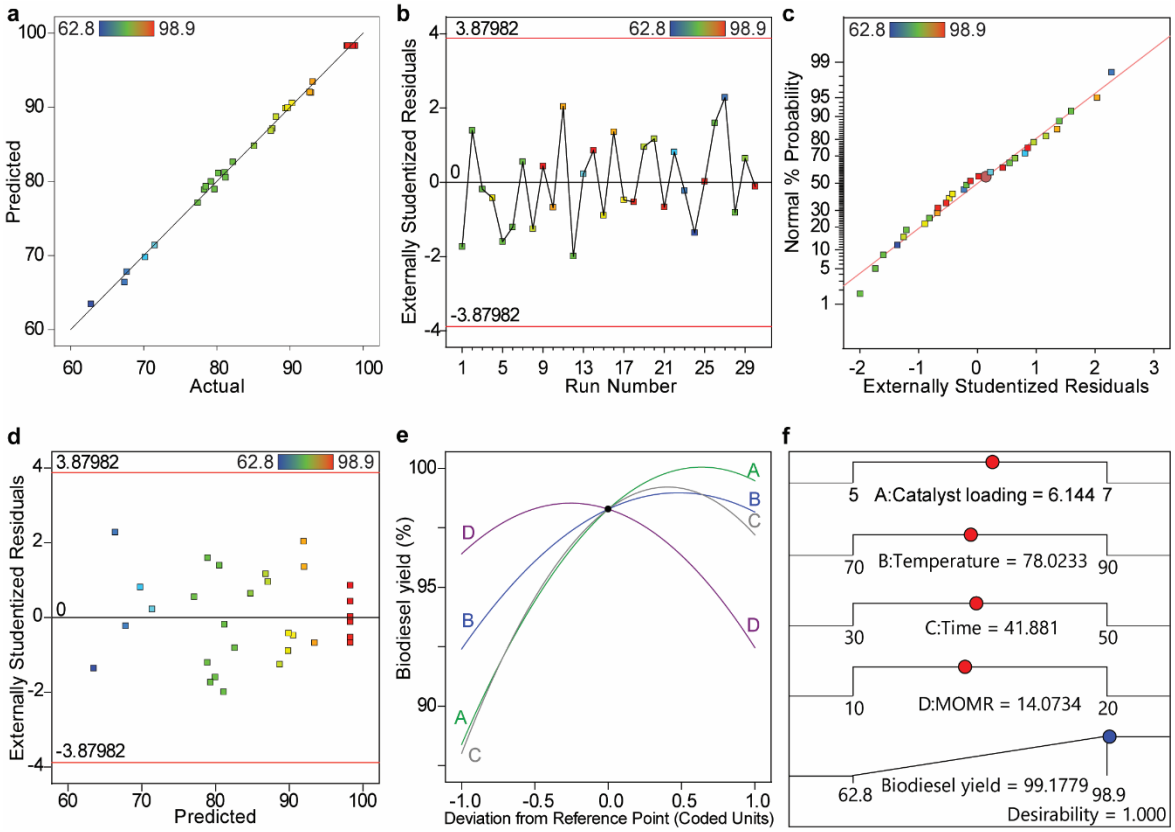

Fig. S6: Diagnostic plots: a) Plot of predicted versus actual % yield of JCO for experiments 1-30 in Table S2, b) Residual differences between predicted and actual yield c) Normal probability plot d) Externally Studentized residuals vs. predicted yield e) Perturbation plot of illustrating factors that profoundly influence biodiesel yield and f) Optimized results for JCOME yield based on the RSM-CCD approach

18. ^{1}H NMR of JCO biodiesel

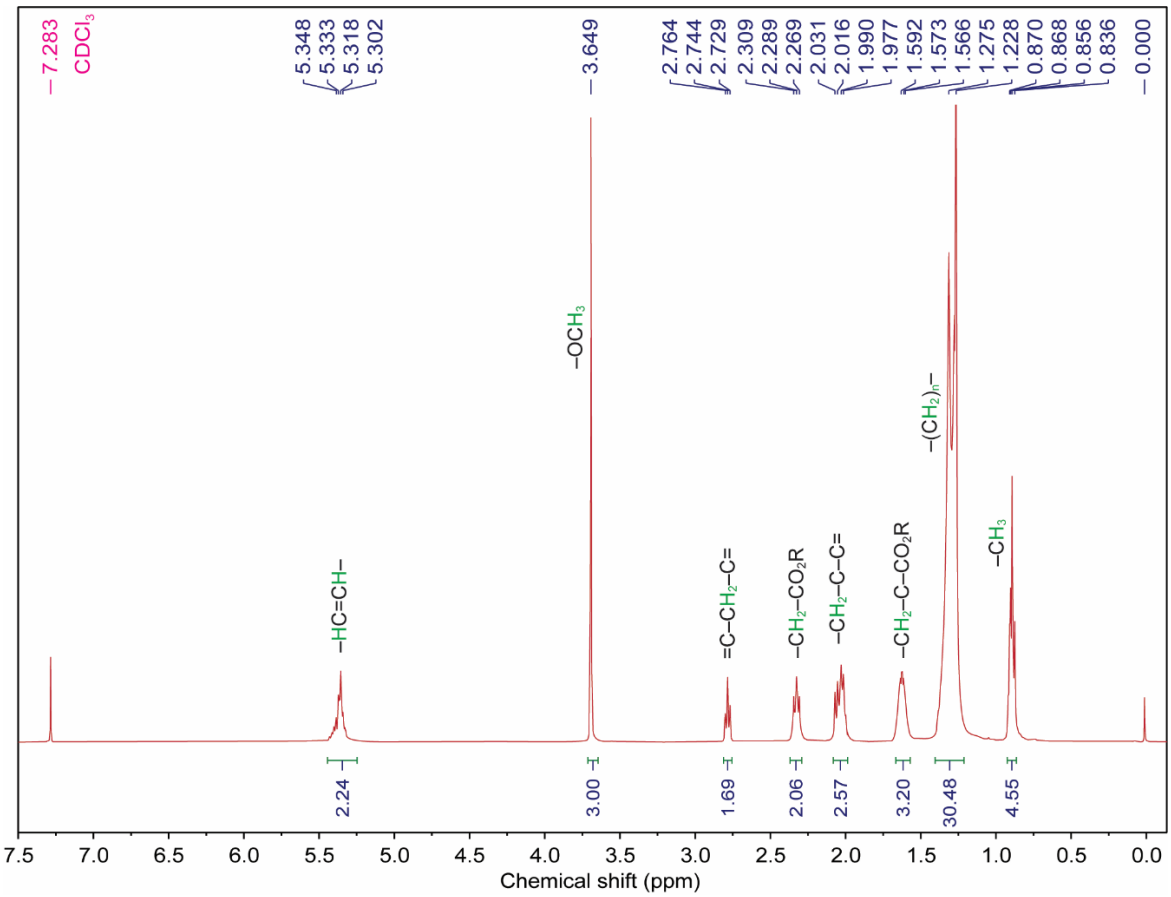

Fig. S7: ^{1}H NMR spectra of JCO biodiesel (400 MHz, $CDCl_3$)

19. ^{13}C NMR of JCO biodiesel

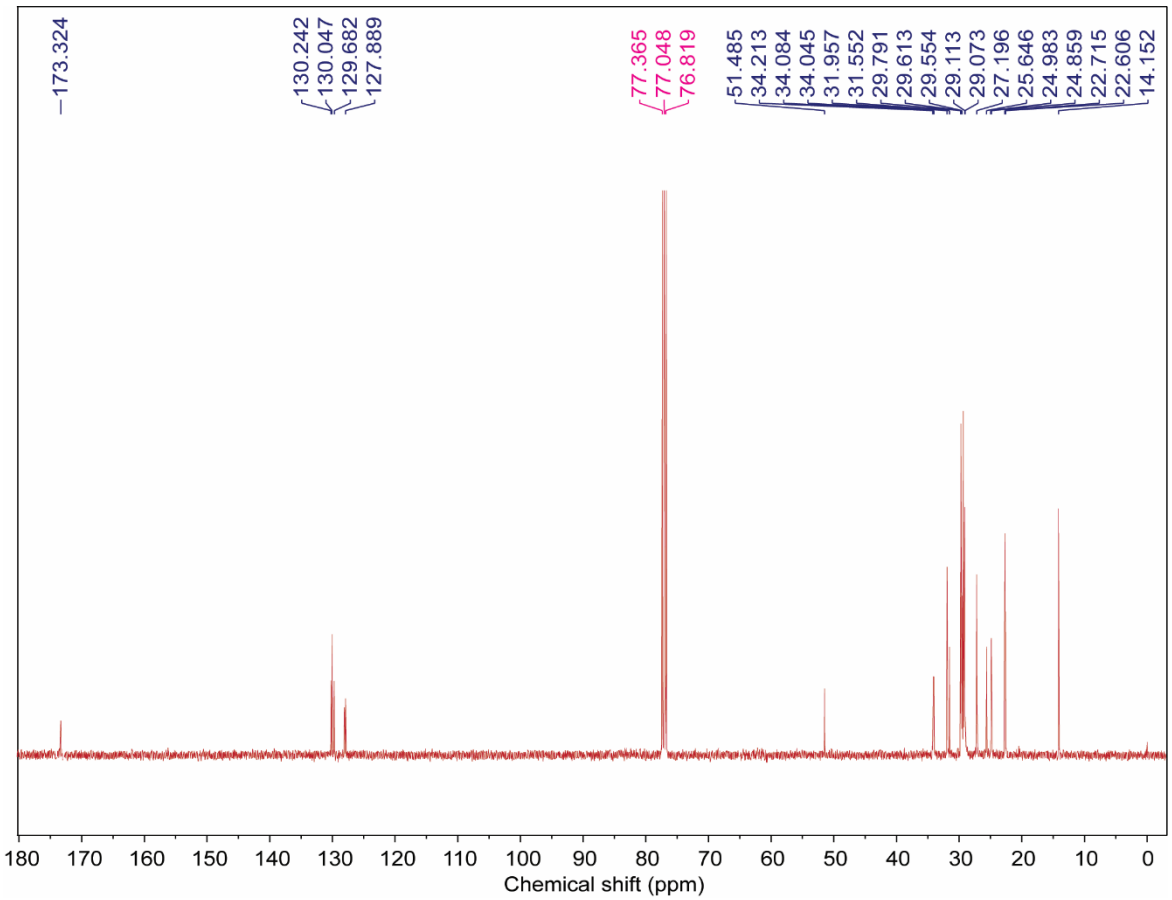

Fig. S8: ^{13}C NMR spectra of JCO biodiesel (100 MHz, $CDCl_3$)

20. GC parameters employed for testing biodiesel

The GC-MS analysis of each sample was carried out on Shimadzu (GC-2030) series GC-MS equipped with Headspace (HS-20) & QQQ Mass spectrometer GC-TQ8040NX. The column was used SH-Rxi-5 SILMS (0.25 X 30 X 0.25). Helium was used as the carrier gas with flow rate of 1.00 ml min^{-1}. The column temperature was initially programmed at 50 °C held for 4 min then increased to150 °C at the rate of 07° held for 4 min then increased to 260 °C at the rate of 07° held for 4 min, through split ratio (30:70) mode. Injector Temperature was 260 °C, Ion source temperature was 220 °C & interface temp was 270 °C. Sample was diluted in ethyl acetate 10:100 v/v and 02 µl injected with a constant temperature of 260 °C through an autosampler injector. The ionization energy was 70 eV and mass range of 40–500 AMU. The management of the GC-MS system, parameter settings for GC and mass spectrometry, and data receipt and processing were performed using Shimadzu Realtime Analysis. The compounds were identified by using NIST library.

21. Gas chromatogram of JCO biodiesel produced

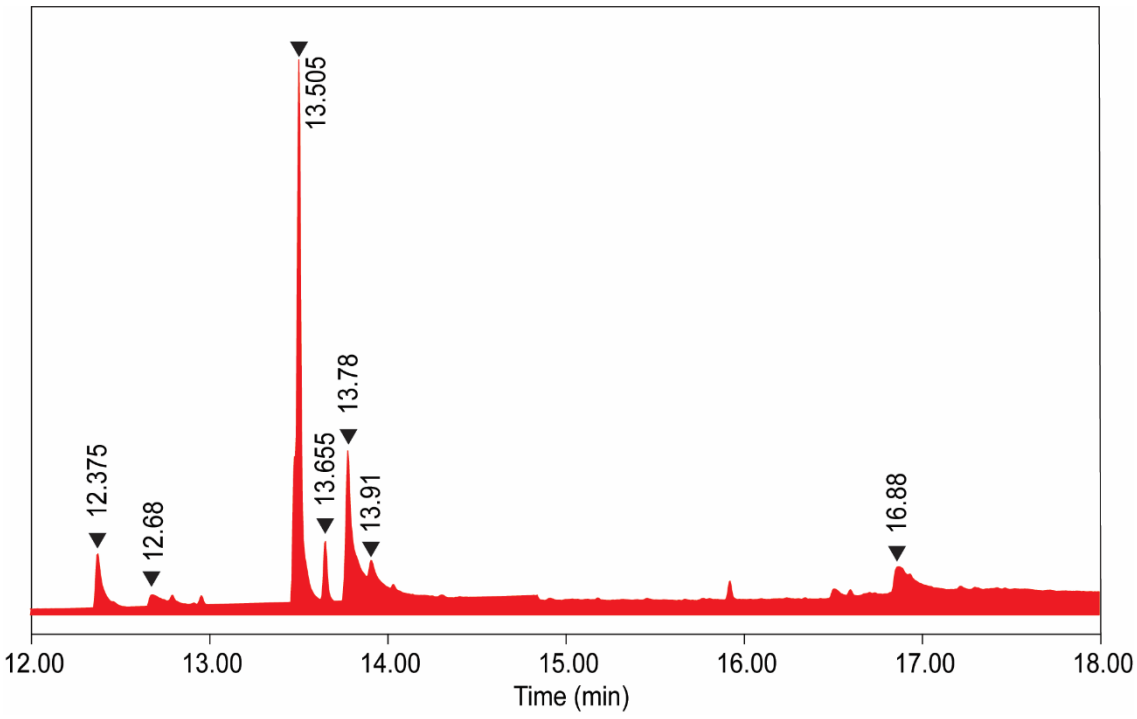

Fig. S9: Gas chromatogram of JCO biodiesel.

22. Chemical composition of obtained JCO biodiesel

Table S8: Chemical composition of the product JCO biodiesel

Peak no.	Retention time (min)	Corresponding acid	Identified component		Area (%)
			IUPAC name	Common name	
1.	12.375	C 16:0	Hexadecanoic acid, methyl ester	Methyl palmitate	5.258
2.	12.68	C 16:1	Hexadecenoic acid, methyl ester	Methyl palmitoleate	2.895
3.	13.505	C 18:1 cis	9-Octadecenoic acid, methyl ester (Z)	Methyl oleate	39.227
4.	13.655	C 18:0	Octadecanoic acid, methyl ester	Methyl stearate	4.568
5.	13.78	C 18:2 cis	9,12-Octadecadienoic acid (Z,Z), methyl ester	Methyl linoleate	18.287
6.	13.91	C18:3	Octadecatrienoic acid (Z,Z,Z), methyl ester	Methyl linoleneate	9.619
7.	16.88	C20:0	Eicosanoic acid, methyl ester	Methyl archidate	20.146

23. Physicochemical properties of generated JCO biodiesel

Table S9: Physicochemical properties of JCO biodiesel

Sl. No.	Properties	Standard	JCO biodiesel[a]	ASTMD6757 limits	EN14212 limits
1	Kinematic viscosity at 40 °C ($mm^2\ s^{-1}$)	ASTMD445	4.85	1.9-6	3.5-5.4
2	Density at 15 °C ($kg\ m^{-3}$)	ASTMD1298	875		860-900
3	Flash point (°C)	ASTMD93	180	>130	>120
4	Iodine value (g iodine/100g)	EN14111	104.6	≤120 max	
5	Cetane no.	ASTMD613	53	≥47	
6	Calorific value (KJ/kg)	ASTMD240	40.24		
7	Acid value (mg KOH/g)	ASTMD664	0.48	<0.79	

24. Plausible esterification and transesterification reaction mechanism of FFA and triglyceride in biodiesel synthesis

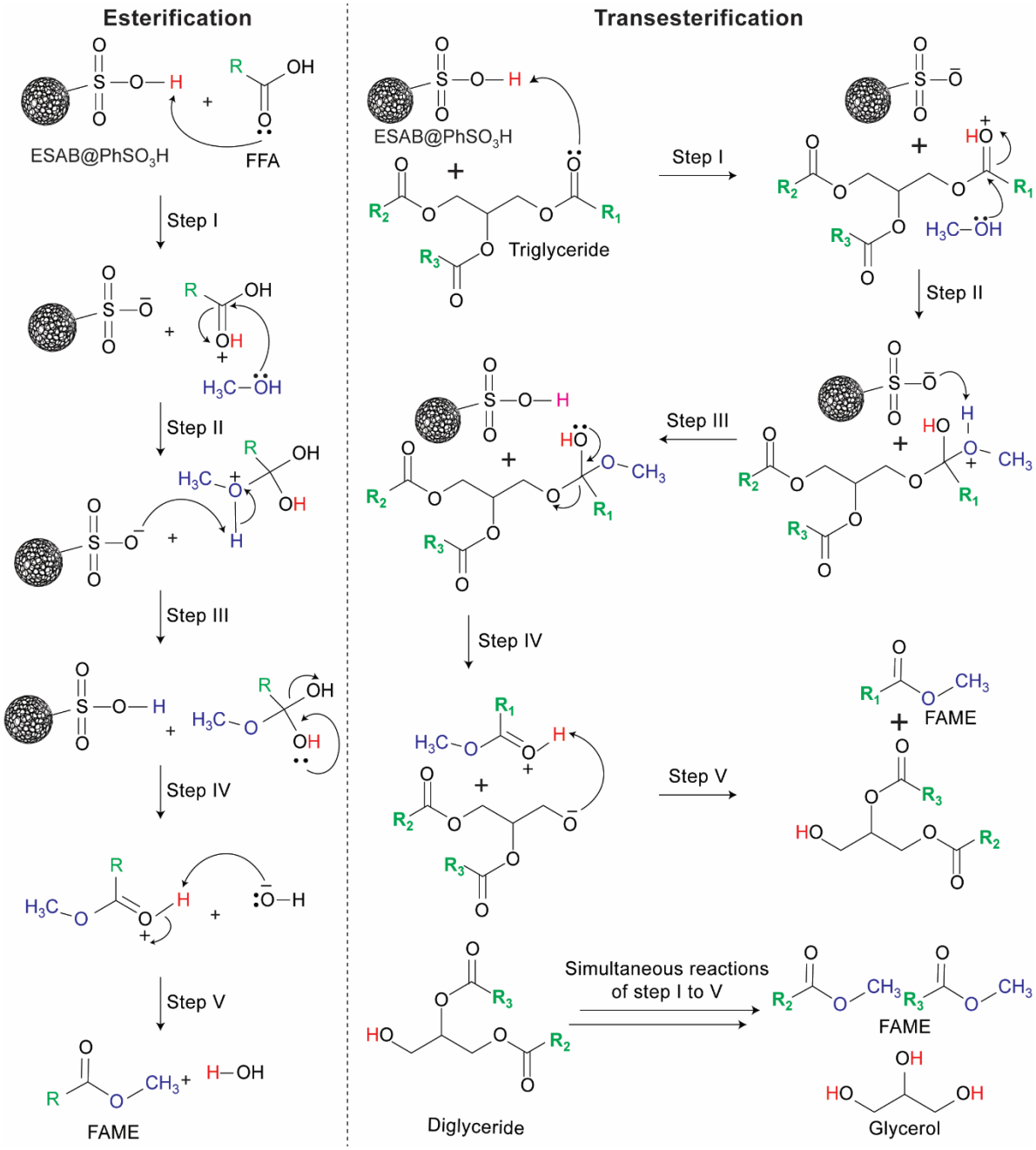

Fig. S10: Esterification and transesterification reaction mechanism catalyzed by sulphonic acid sites of ESAB@$PhSO_3H$.

25. $\Delta G^{\ddagger}$ values at different temperatures

Table S10: Thermodynamic parameters for JCO transesterification using ESAB@PhSO$_3$H catalyst

Temperature (K)	$\Delta G^{\ddagger}$ (kJ mol^{-1})	$\Delta H^{\ddagger}$ (kJ mol^{-1})	$\Delta S^{\ddagger}$ (J K^{-1} mol^{-1})
323	88.14		
333	90.06		
343	91.97		
353	93.88	26.34	–191.34

26. ^{13}C-CP-MAS NMR spectra of the spent catalyst

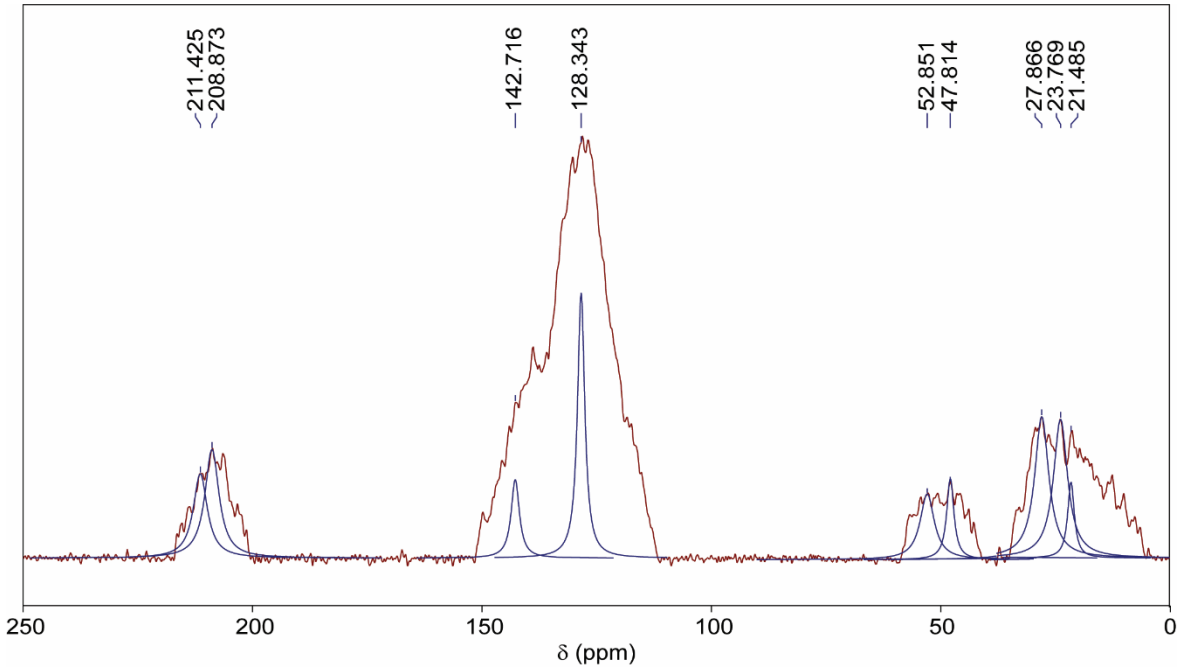

Fig. S11: ^{13}C-CP-MAS NMR spectra of the spent catalyst displaying sulfonate ester formation.

27. EDS spectra and elemental composition of spent catalyst

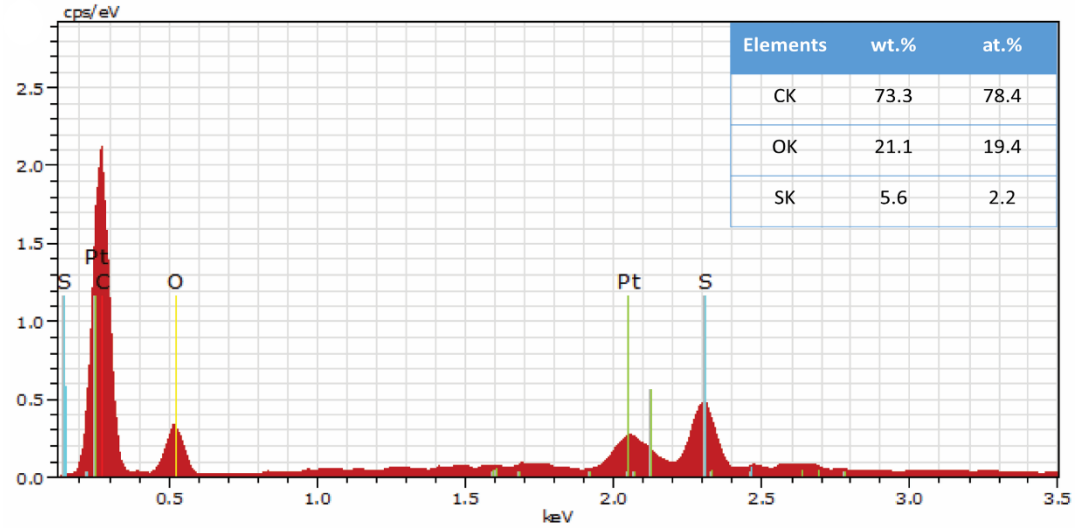

Fig. S12: EDS spectra with elemental composition table (inset) of spent ESAB@PhSO$_3$H catalyst over ten successive runs.

28. Comparison of performance of present catalyst with previously reported hydrophobic catalysts in biodiesel production

Table S11: Comparative study of different hydrophobic catalysts and their application in biodiesel production

Sl. No.	Catalyst	Hydrophobic agent	Surface area ($m^2 g^{-1}$)	Contact angle (◦)	Conditions[a]	Biodiesel yield (%)	Reusability[f]	Ref.
1.	10SA/UiO-66(Zr)	Stearic acid	1150	107.5	39:1, RT, 6, 240	94.5	6, 83	[3]
2.	4.27 wt. % B-p NaphSO$_3$H	p-NaphSO$_3$H	261.2	123	10:1, 60, 10, 600	96.7	5, 88.5	[4]
3.	FDCA/SA-HF	Stearic acid	1080	131.5	19.5:1, 49, 4.1, 570	98.6	6, 90	[5]
4.	FnmS-PIL	Organosilane $CH_3CH_2Si(OC_2H_5)_3$	128	115.4	17:1, 75, 4, 180	95.3	5, 87.5	[6]
5.	6.33 wt.% B-PhSO$_3$H	-	112.1	114	10:1, 60, 1, 600	93	5, 86.1	[7]
6.	HSCA 0.5	Tertbutyl aniline	3397.58	115	2:1[b], 80, 1, 180	71.62[e]	NR	[8]
7.	SSAC@PhSO$_3$H	Caprylic acid	1461	163.4	15:1[c], 80, 5, 40	98.8	9, 86.8	[9]
8.	OP-AC@SO3H-Si	Hexamethyldisilazane	355.09	154	24:1, 99.3, 4.2, 142.2	99.1	9, 90.3	[10]
9.	ESAB@PhSO$_3$H	1-Bromododecane	1256	167.6	15:1[c], 80, 6, 40	98.7	9, 89.6	**Present work**

[a]Methanol: Oleic acid molar ratio, temperature (◦C), catalyst loading (wt. %), time (min); [b]Ethanol: Acetic acid molar ratio; [c]Methanol: JCO molar ratio; [d]Methanol: WCO molar ratio; [e]Conversion; [f]No. of cycles reused, Biodiesel yield (%); RT-Room Temperature; NR-Not Reported

SA/ UiO-66(Zr): Stearic acid grafted UiO-66(Zr); FDCA/SA-HF: 2.5-Furandicarboxylic acid/ Stearic Acid-Hafnium chloride

29. Study on life cycle cost analysis

Cost estimation of the synthesized catalyst

Table S12: LCCA of stepwise catalyst preparation

Step	Description	Amount
Cost of starting material (SMC)	Cellulose	$5.472
Cost of chemicals in activation, sulfonation and etherification for catalyst preparation (CRC)	Cost of chemicals (n-bromododecane, potassium iodide, potassium carbonate, 4-aminobenzenesulfonic acid, H_3PO_2, $ZnCl_2$, HCl, $NaNO_2$, ethanol, acetone, water)	$53.489
Cost for hydrothermal carbonization (CHC)	Time (h) × units consumed × cost per unit= 20 × 1 × $0.063	$1.26
Drying cost (DC)	Before pyrolysis, for the removal of water	$0.6
Carbonization cost (CC) = IEC (IEC = inert environment creation costs) + PC (Pyrolysis cost)	IEC = N_2 flow = $0.6 PC = Time (h) × units consumed × cost per unit= 2 × 1 × $0.063 = $0.126 CC = $0.6 + $0.126	$0.726
Cost for sulfonation (CS)	CS = Time (h) × units consumed × cost per unit= 3 × 0.5 × $0.063	$0.094
Cost for etherification (CE)	CE = Time (h) × units consumed × cost per unit= 24 × 1 × $0.063	$1.512
Net cost involved	SMC+CRC+CHC+DC+CC+CS+CE = $5.472+ $53.489+ $1.26+ $0.6+ $0.726+$0.094+ $1.512	$63.153
Total cost/kg	= Net cost + running charges (15% of the net cost) = $63.153 + $9.473	$72.626
Final cost of 1 kg catalyst after 15 times of reuse	= one-time preparation cost/no. of cycles towards catalyst reusability = $72.626/15	$4.842

Cost estimation of JCO biodiesel production

Table S13: LCCA of stepwise biodiesel production

Step	Description	Cost
Cost of feedstock	*Jatropha curcas* oil	$0.005
Cost of catalyst for 1 kg biodiesel	Required amount × cost of preparation of 1kg catalyst = 0.063 × $4.842	$0.305
Methanol required for biodiesel production	Required amount × cost per litre = 0.115 × $0.32 (unreacted methanol is being reused after each cycle)	$0.039
Biodiesel production cost	(Time duration for esterification (h) × units × per unit cost) = 0.7× 0.5× $0.063	$0.022
Cost for 1kg biodiesel production		$0.371
Overhead cost[a]	15% of the net cost	$0.056
Overall cost for 1kg biodiesel production		$0.427
Overall cost for 1L biodiesel production	Density × Cost for 1kg biodiesel production= 0.875 × 0.427	$0.374

[a]Overhead cost in biodiesel production = 15 % of the net charge and includes indirect expenses such as administrative, utility, and facility costs.

30. Sensitivity analysis of the impact of catalyst recycling on the LCCA result

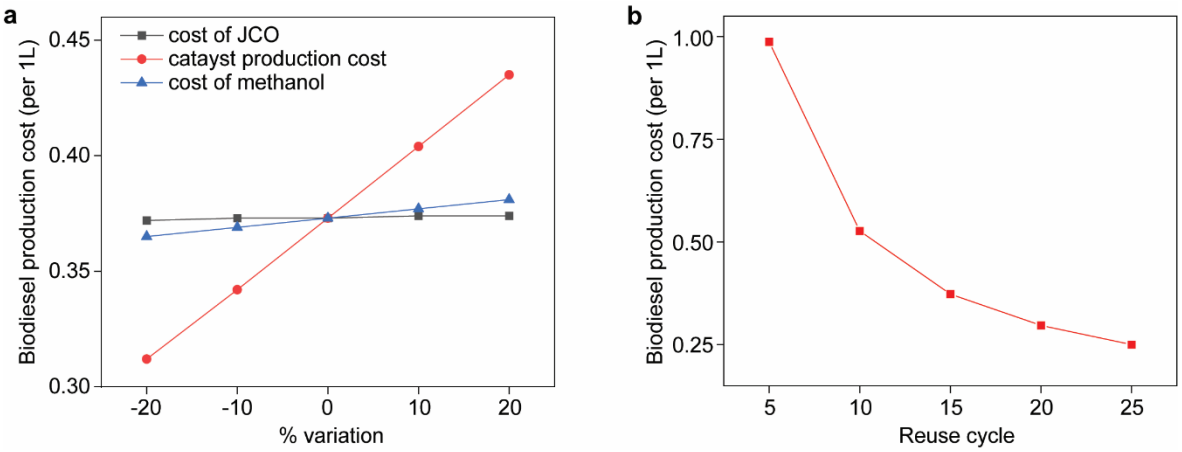

Fig. S13: The impact of JCO price, catalyst production cost, methanol price (a) and recyclability (b) on the biodiesel production cost

31. Environmental impact assessment of ESAB@PhSO$_3$H catalyst in biodiesel synthesis

Table S14: Environmental impact assessment in1 kg biodiesel production from ESAB@PhSO$_3$H catalyst

Sl No.	Impact category	Unit	Catalyst preparation (a)	Biodiesel production (b)			Total [a+b]
				JCO	Methanol	Electricity	
1.	Abiotic depletion	kg Sb eq	6.51E-6	1.1E-5	3.24E-7	1.42E-6	1.93E-5
2.	Global warming	kgCO_2 eq	0.457	1.45	0.188	0.207	2.3
3.	Human toxicity	kg 1,4-DB eq	2.97	14.2	0.4	0.311	17.9
4.	Fresh water aquatic ecotoxicity	kg 1,4-DB eq	0.427	1.41	0.0649	0.11	2.01
5.	Marine aquatic ecotoxicity	kg 1,4-DB eq	1.21E3	5.04E3	187	141	6.58E3
6.	Terrestrial ecotoxicity	kg 1,4-DB eq	0.0177	0.57	0.00272	0.00176	0.592
7.	Photochemical oxidation	kg C_2H_4 eq	0.000222	0.000205	0.000114	2.41E-5	0.000565
8.	Acidification	kg SO_2 eq	0.00168	0.0275	0.000358	0.000341	0.0298
9.	Eutrophication	kg PO_4^{3-} eq	0.000766	0.0102	0.000124	6.82E-5	0.0112

This study employed the CML-IA baseline method with long-term time horizons to evaluate key environmental impact categories, including abiotic depletion, global warming, human toxicity, ecotoxicity, acidification, and eutrophication (**Table S14**). The global warming potential (GWP) associated with JCO biodiesel, including catalyst synthesis, was calculated as 2.3 kg CO_2-eq per kg of biodiesel. While this exceeds values reported for vegetable oils-based biodiesel, viz. soybean (0.6 kg CO_2-eq), sunflower (1.24 kg CO_2-eq), cottonseed oil (1.475 kg CO_2-eq); it remains lower than some previously reported values for inedible oil derived biodiesel such as JCO (3.17–11 kg CO_2-eq) and WCO (27.2–299.6 kg CO_2-eq) [11]. Compared to studies by Carvalho et al. [12], Ao et al. [13], the current system demonstrated lower eutrophication, abiotic depletion, and acidification potentials. However, human and marine aquatic toxicity impacts were notably higher, which is likely attributable to specific processing routes and catalyst synthesis strategies. These results highlight the critical role of feedstock type and catalyst preparation methodology in determining the environmental profile of biodiesel production.

32. Network representation for production of 1 kg biodiesel showing significant damage impact by catalyst

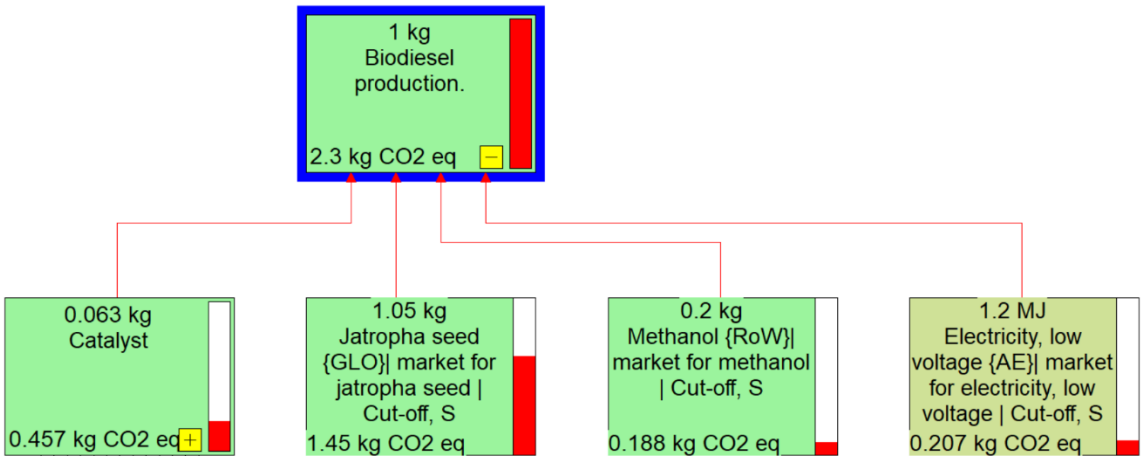

Fig. S14: Network representation, highlighting the global warming impact by each stage involved in the process of production of 1 kg of biodiesel using ESAB@$PhSO_3H$ catalyst.

33. Percentage variation due to potential environmental impact assessment evaluated using CML- IA baseline V3.11/EU25

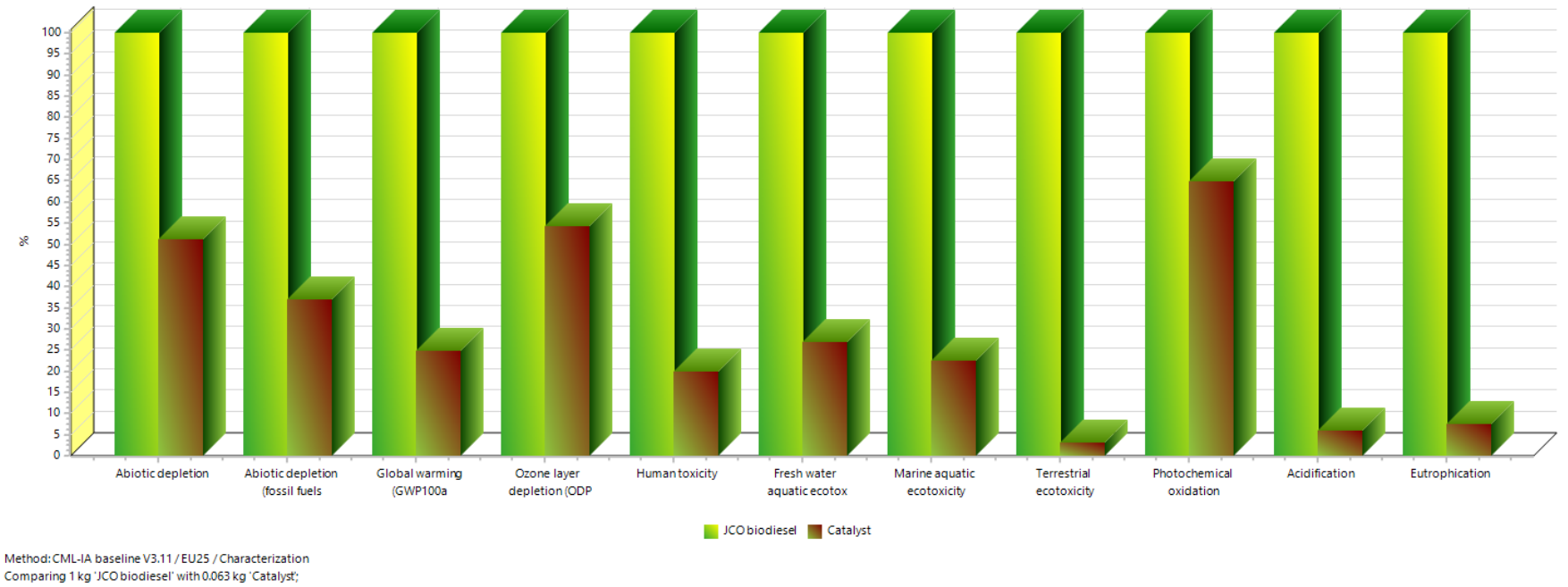

Fig. S15: Percentage variation in potential environmental impact assessment for producing 1 kg biodiesel using ESAB@PhSO$_3$H catalyst as assessed with CML-IA baseline version 3.11.

References:

1 X. Y. Liu, M. Huang, H. L. Ma, Z. Q. Zhang, J. M. Gao, Y. L. Zhu, X. J. Han and X. Y. Guo, *Molecules*, 2010, **15**, 7188–7196.

2 Y. Ning and S. Niu, *Energy Convers. Manag.*, 2017, **153**, 446–454.

3 A. S. Abou-Elyazed, Y. Sun, A. M. El-Nahas and A. M. Yousif, *RSC Adv.*, 2020, **10**, 41283–41295.

4 Y. Zhong, Q. Deng, P. Zhang, J. Wang, R. Wang, Z. Zeng and S. Deng, *Fuel*, 2019, **240**, 270–277.

5 Y. Li, K. Zhu, Y. Jiang, L. Chen, H. Zhang, H. Li and S. Yang, *Fuel Process. Technol.*, 2023, **239**, 107558.

6 H. Zhang, H. Li, H. Pan, A. Wang, S. Souzanchi, C. (Charles) Xu and S. Yang, *Appl. Energy*, 2018, **223**, 416–429.

7 H. Li, Q. Deng, H. Chen, X. Cao, J. Zheng, Y. Zhong, P. Zhang, J. Wang, Z. Zeng and S. Deng, *Appl. Catal. A Gen.*, 2019, **580**, 178–185.

8 A. S. Suryandari, T. Nurtono, W. Widiyastuti and H. Setyawan, *ACS Omega*, 2023, **8**, 27139–27145.

9 A. Das, C. Guchhait, B. Adhikari, K. Saikia, D. Shi, H. Li and S. L. Rokhum, *Adv. Funct. Mater.*, 2024, **34**, 2406262.

10 S. Ao, S. Zhang, P. K. Karoki, R. Kousika, G. A. Goenaga-Jimenez, T. McCoy, W. Wang, N. Han, C. G. Yoo, C. Guchhait, B. Adhikari, X. Meng, T. A. Zawodzinski, S. L. Rokhum and A. J. Ragauskas, *Green Chem.*, 2025, **27**, 13789–13803.

11 K. Srikumar, Y. H. Tan, J. Kansedo, I. S. Tan, N. M. Mubarak, M. L. Ibrahim, P. N. Y. Yek, H. C. Y. Foo, R. R. Karri and M. Khalid, *Biomass and Bioenergy*, 2024, **185**, 107239.

12 F. S. Carvalho, F. Fornasier, J. O. M. Leitão, J. A. R. Moraes and R. C. S. Schneider, *J. Clean. Prod.*, 2019, **230**, 1085–1095.

13 S. Ao, S. P. Gouda, M. Selvaraj, R. Boddula, N. Al-Qahtani, S. Mohan and S. L. Rokhum, *Energy Convers. Manag.*, 2024, **300**, 117956.